CONF-890665--12

HERMES-III POSITIVE POLARITY EXPERIMENT*

Received by OSTI

JUN 1 5 1989

D. L. Johnson, J. A. Alexander, J. J. Ramirez, J. P. Corley
G. J. Denison, J. W. Poukey, T. R. Lockner, S. E. Rosenthal, C. Ruiz
Sandia National Laboratories
Albuquerque, New Mexico 87185

SAND--89-0071C

DE89 013153

Abstract

Hermes-III is a 22-MV, 730-kA, 40-ns electron beam linear induction accelerator with a magnetically insulated transmission line (MITL) adder used to produce bremsstrahlung radiation. Hermes-III has been operated in a reverse polarity mode to study possible applications of the Hermes-III technology to Sandia National Laboratories' Inertial Confinement Fusion Program. To accomplish the polarity reversal, the twenty induction cavities were rotated and the MITL was reinserted in the cavities. The Marx generators and the pulse forming networks were operated in negative polarity as before. The accelerator was operated at three levels: 50%, 80%, and 95% of full voltage and with two diode configurations. Data is presented on the operation of the positive polarity MITL adder, on the effects on the cavities, and on the operation of a pinched-beam, ion diode.

Introduction

The 16-TW, Hermes-III accelerator is operating reliably[1,2] as a source of bremsstrahlung radiation for Sandia National Laboratories' Weapons Effects Program. The technology employed in Hermes III is the basis for a conceptual design of a light ion beam driver[3] for a Laboratory Microfusion Facility (LMF). This driver consists of thirty-two 32-MV, 1.2-MA ion beam accelerators. In the ion accelerator, the MITL must operate with center conductor at positive polarity, with respect to the outer conductor and be terminated by an extraction ion diode. The operation of the positive polarity MITL adder is a critical issue in the accelerator design. Preliminary analysis indicated that the positive adder had more complex electron flow and was less efficient than the negative adder.

To provide information on the operation of the adder and on its interaction with the linear induction cavities, Hermes III was operated in a positive polarity configuration.

The positive configuration could also provide a test bed for ion beam generation, focusing, and transport experiments. To accomplish the polarity reversal. the MITL was removed. the twenty cavities were rotated 180 degrees, and the MITL reinserted through the cavities. The Marx generators and pulse forming networks were operated in negative polarity as before. Two diode configurations were used: An inverse electron beam diode and a pinched-beam ion diode. The ion diode was used to accelerate protons and lithium ions.

Experimental Description

A cross sectional view of the Hermes-III cavity adder and MITL is shown in Fig. 1. Monitors are located at each of the cavity spools within the adder (positions 1 to 4) and along the extension MITL (positions 5 to 9). The adder portion is 12.6-m long, with a 6-m MITL extension terminated by the diode. Voltage is applied to the MITL at each of the cavities. Figure 2 is drawing of the electron beam diode that was used for most of the shots. Figure 3 is a drawing of the pinched-beam, ion diode that was used for ion shots. Current measurements were made at each cavity and on the inner and outer conductors at each spool location and on the extension MITL. Peak voltage measurements were made at each cavity. Peak output voltages were determined by range measurements in filtered CR-39 nuclear tracking film detectors.[4]

The total machine current is carried on the center conductor of the MITL adder, the boundary current flows on the outer conductor, and a sheath current flows between the inner and outer conductors. Electrons flowing in the sheath current have varying kinetic energies, determined by the potential difference between the anode and cavity from which they are emitted. These sheath current electrons represent an energy loss if they are not recaptured to the surface from which they were emitted.

Since the sheath current increases down the length of the adder section, the boundary current decreases. Within the adder section, the cavity current is the same as the boundary current. The cavity current is inversely proportional to the load impedance for the cavities. Therefore, the load impedance for each cavity must increase down the length of the adder; it then follows that the cavity output voltage would also increase down the length of the adder section. Table 1 shows the results of a simplified model of the Hermes-III adder section where the sheath current was assumed to increase linearly from 0-30% of the total current along the length of the adder.

Table 1. Calculated voltages (in MV), current (in MA), and power (in TW) for a Hermes-III cavity adder with a sheath current assumed to increase linearly from 0-30% of the total current.

cav #	cav volts	cav amps	cav power	sum volts	sheath power
1	0.950	0.760	0.722	0.950	0.011
2	0.965	0.748	0.722	1.915	0.023
3	0.980	0.736	0.721	2.895	0.035
4	0.995	0.724	0.720	3.890	0.047
5	1.010	0.712	0.719	4.900	0.059
6	1.025	0.700	0.717	5.925	0.071
7	1.040	0.688	0.716	6.965	0.084
8	1.055	0.676	0.713	8.020	0.096
9	1.070	0.664	0.710	9.090	0.109
10	1.085	0.652	0.707	10.175	0.122
11	1.100	0.640	0.704	11.275	0.135
12	1.115	0.628	0.700	12.390	0.149
13	1.130	0.616	0.696	13.520	0.162
14	1.145	0.604	0.692	14.665	0.176
15	1.160	0.592	0.687	15.825	0.190
16	1.175	0.580	0.682	17.000	0.204
17	1.190	0.568	0.676	18.190	0.218
18	1.205	0.556	0.670	19.395	0.233
19	1.220	0.544	0.664	20.615	0.247
20	1.235	0.532	0.657	21.850	0.000

Available power = 14.44 TW
Total sheath power = 2.37 TW
Power from cavities = 14.00 TW
Net power = 11.63 TW
Efficiency = 80.5%

The sheath power is the sheath current at a cavity times the voltage at that location in the MITL (i.e., power that would be lost if these electrons were accelerated to the anode), and the available power is the power capable of being delivered to a matched impedance load. The efficiency is the power from the cavities, less the sheath power, divided by the total available power. This is a greater efficiency than would be obtained if a 30% current loss at full voltage were assumed.

Experimental Results

For the experiment, Hermes III was operated at three levels: half voltage for 19 shots, full voltage for 5 shots, and approximately 80% voltage for 26 shots. At each level, the total current along the inner conductor of the MITL adder remained constant within measurement accuracy indicating negligible loss of sheath current. The boundary current decreased to 60-70% of the total current at the end of the adder. This fraction was the same for the three operating levels. In the extension MITL, there was a marked decrease in the boundary current; the magnitude of this drop in boundary current was a function of the operating level. Figure 4 is a normalized plot of the measured peak currents for the full and half operating points with the electron beam load. Peak total currents for the two cases are 820 kA and 390 kA, respectively. The boundary current within the adder decreases nearly linearly to ~65% of the total current and is the same for the two operating levels. However, the fraction of boundary current in the extension MITL depends on the operating voltage.

For two shots, a 10-cm by 10-cm nylon mesh screen was placed on the anode surface at two points on the electron beam diode. CR-39 range detectors were placed opposite these locations on the cathode surface (see Fig. 2). The screen serves as a source of protons when it is struck by electrons. These protons are then accelerated across the A-K gap. For the 90% operating point, the CR-39 indicated 12 MeV protons at position 1 and 18 MeV protons at position 2 on the same shot. The CR-39 detector at position 1 may have been located such that protons greater than 12 MeV missed the detector due to magnetic sweeping of the protons.

Six shots were taken with the pinched-beam ion diode shown in Fig. 3, four with a nylon mesh proton source and two with a lithium-fluoride coated stainless steel lithium source. Energetic lithium ions were measured by activation, neutron time-of-flight (TOF), and nuclear threshold techniques. The activation and neutron TOF require neutrons that are produced by the d(^{7}Li,n) reaction. Lithium ions are allowed to strike a thick deuterated carbon target, CD_2. The energy of the neutrons produced is $\geq$ 14 MeV. In the activation method, the neutrons that are produced strike a Cu slug of known weight where the reaction ^{63}Cu(n,2n) produces ^{62}Cu that decays by β^+ ($\tau_{1/2}$ = 9.74 min). By measuring the activity, counts per minute, and comparing this value with a calibrated yield (cpm/gm of Cu per Li ion), an estimate of the number of Li ions striking the detector is determined.

It is estimated that on the two lithium shots a minimum of 10 kJ of lithium ions were produced. Confirmation that lithium ions produced the neutrons is seen in the spectra from a neutron TOF detector placed 15 m from the source. A signal attributed to neutrons indicated neutrons with energies above 14 MeV. Because of saturation problems at the detector from bremsstrahlung radiation, it was not possible to determine the peak lithium voltages. An activation threshold technique also confirmed the production of lithium ions. The reaction was $p(^7Li,n)^7Be$ that has a threshold of 13.5 MeV. After each shot, the activated CH_2 target sample was placed near a NaI detector in order to observe the 478-keV gamma rays emitted from the decay of Be. The measurements confirmed lithium beams with energies $\geq$13.5 MeV.

Current measurements by the ion diode B-dot monitor, shown in Fig. 3, showed a peak current of 90 kA for a proton shot and 73 kA for a lithium shot. These current measurements are a lower bound to the ion current since the B-dot monitor will measure net current. The lithium ions, that are produced in the A-K gap, should be singly ionized, and the current reduced from the proton case by a factor of 2.65, the square root of their mass ratio. However, when the ions pass through the 0.0013-cm thick aluminized-mylar cathode foil, they are stripped of electrons and become triply ionized, thus increasing this current by a factor of three. Activation of the stainless-steel witness plate was evident with the proton shots, but little activation was seen on the lithium shots indicating little proton current in the lithium shots.

Theory and Numerical Simulation

Some basic questions about magnetically insulated flow in the positive-polarity Hermes-III accelerator have been addressed by simple physical models in conjunction with numerical simulation using the electromagnetic, relativistic, particle-in-cell code MAGIC.[5] These questions relate primarily to the consequences of multiple-cathode electron emission in magnetically insulated transmission lines. The noteworthy feature of positive-polarity operation, for which the outer electrode is the cathode, is that the 20-radial power feeds of Hermes III divide the cathode surface into 20 separate sections. Hence, the final MITL is populated by what can be considered as 20 distinct classes of electrons. Each class is defined by the potential difference between the anode and the cathode from which its members were emitted. In negative polarity there is only one class of electrons since all electrons are emitted from the same cathode, the uninterrupted inner conductor of the coaxial line.

Because each successive class of electrons is emitted with a different set of canonical momenta and total energies, a consideration of the allowed momentum-energy values for electrons in the flow[6] in the Hermes-III final MITL shows that the electrons injected into the flow from the various adder-section cathodes must necessarily travel very close to the extension MITL anode.

Figure 5 shows electron trajectory maps from a realistic-pulse MAGIC simulation at 22 ns into the pulse. At this time, the flat top of the input voltage has been reached at each of the feeds and the system is still line-dominated. The maps compare the spatial distribution of electrons that were emitted from all of the adder-section cathodes (Fig. 5a) with that of the electrons that were emitted from the cathode of the final MITL (Fig. 5b). We call the flow that is constituted by the electrons emitted from the final-MITL cathode Insulated-Indigenous-Flow (IIF). The electrons injected into the final MITL from the adder basically fill in the gap between the IIF and the MITL anode. The injected flow, together with the IIF, comprise what we call Full-Gap-Flow (FGF). A simple prescription exists for the calculation of line voltage from the final-MITL total (anode) and boundary (cathode) current waveforms based on FGF. There is some radial mixing of electron classes in the final MITL flow, but a description of the flow as radially layered is reasonably appropriate and allows us to calculate the line voltage from the IIF as well.

The variation of simulation anode and cathode currents with axial position plotted in Fig. 6 shows how the portion of the total current carried by the electrons (total - boundary) increases with increasing number of electron classes in the flow. Figure 7 shows how the percentage of the total current, $100\ (1-I_c/I_A)$, carried by the electron flow increases with position for Hermes-III shot 619 (full-voltage shot), and for the corresponding MAGIC simulation. The percentage of electron flow that is calculated from the simulation voltages and anode currents using the FGF model is also included for comparison. The FGF description is expected to be valid beginning axially at monitor position 4, Fig. 7.

When the FGF model is valid, the MITL voltage can be calculated very simply from the line currents by the following expression:

$$V = (Z_0/2)\,(I_A^2 - I_C^2)^{1/2},$$

which is based on pressure balance and assumes only that the flow extends across the whole gap, and that the electron density profile of this flow is radially uniform. The uniform density assumption is not restrictive since the voltage is insensitive to the density profile. The FGF voltage expression underestimates the voltage when the flow does not extend across the whole gap. The single-cathode MITL voltage-current relationship based on pressure balance is[7-9]

$$V = Z_0\,(I_A^2 - I_C^2)^{1/2} - (\dot{m}c^2/2e)\,(I_A^2/I_C^2 - 1).$$

This expression can be applied to the multiple-cathode positive-polarity Hermes III if a modified I_A is used. This modified anode current includes only the IIF and, therefore, is given by the full anode current downstream of the last radial feed less the flow current just upstream of the last feed. Both the experiment and the simulations indicate that there is insignificant loss along the system, so the modified anode current becomes the cathode current just upstream of the last radial feed. The IIF and FGF calculated voltages for Hermes III shot 619 are presented in Fig. 8. The agreement indicates that both IIF and FGF assumptions are correct if the current measurements are accurate. The 16-MV peak is about 20% less than what would be expected from extrapolating the range-filtered CR-39 measurements made on lower voltage shots.

Conclusions

Efficient current transport was measured in the positive polarity MITL adder experiment. High energy ions were detected indicating that the high voltage pulse was transported efficiently to the end of the extension MITL. Continued research is planned to further investigate the interaction between the MITL adder and the induction cavities.

Theoretical considerations pertaining to multiple-cathode MITLs and an analysis of numerical simulations and of Hermes-III current measurements indicate that electron flow, on the average, occupies the entire anode-cathode gap of the final MITL of Hermes III when operated in the positive polarity. FGF occurs even though the transfer of anode current from beginning to end of the accelerator is near 100% efficient. We are presently investigating the implications of FGF for coupling energy to an applied-B ion diode.

References

1. J. J. Ramirez, et al., "The Hermes-III Program," in Proceedings of the 6th IEEE Pulsed Power Conference, Arlington, VA, 1987, p. 294.

2. J. J. Rmairez, et al., "Performance of the Hermes-III Gamma Ray Simulator, in these proceedings.

3. D. L. Johnson, et al., "A Conceptual Design For an LMF Accelerator Module", to be published, 1989 Particle Accelerator Conference, Chicago, IL, March 1989.

4. J. Bailey, et al., Bull. Am. Phys. Soc., 32, p. 1873, (1987).

5. B. Goplen, R. E. Clark, J. McDonald, and W. M. Bollen, Mission Research Corporation Report No. MCR/WDC-R-068, Alexandria, VA, Sept. 1983; T. D. Pointon, SAND88-0982 UC-28, June 1988.

6. C. W. Mendel, D. B. Seidel, and S. A. Slutz, Phys. Fluids 26(12), 3628 December 1983.

7. C. W. Mendel, Jr., D. B. Seidel, and S. E. Rosenthal, Laser and Particle Beams, 1(3), 311 (1983).

8. P. A. Miller and C. W. Mendel, Jr., J. Appl. Phys., 61(2), 529 (1987).

9. S. E. Rosenthal and C. W. Mendel. Jr., Particle Beam Fusion Progress Report July 1985 through December 1985, SAND86-0016, p. 59.

Figure Captions

1. Cross section of the Hermes-III cavity adder and MITL.

2. Electron beam diode.

3. Ion diode.

4. Normalized total and boundary currents for high voltage (squares) and low voltage (triangles) shots. Position 5 is just beyond the adder. The cavity currents (circles) match the bound current in the adder section.

5. Electron trajectory maps from MAGIC at 22 ns into the full-voltage, realistic-pulse Hermes-III simulation contrast the injected flow with the Insulated-Indigenous-Flow of the final MITL. Both flows are present in the simulation and together comprise the Full-Gap-Flow.

6. Plot of mid-pulse total and boundary currents vs. axial position from the full-voltage Hermes-III simulation. The location numbers correspond to those of the experiment.

7. Comparison of full-voltage Hermes-III electron flow currents as a percentage of the total current from computer simulation, shot 619, and FGF model.

8. Comparison of calculated voltages for Hermes shot 619. The IIF voltage was calculated from cathode currents just upstream and downstream of the 20th feed; the FGF from the anode and cathode currents just downstream of the 20th feed.

*This work was supported by the U.S. Department of Energy under Contract DE-AC04-76DP00789.

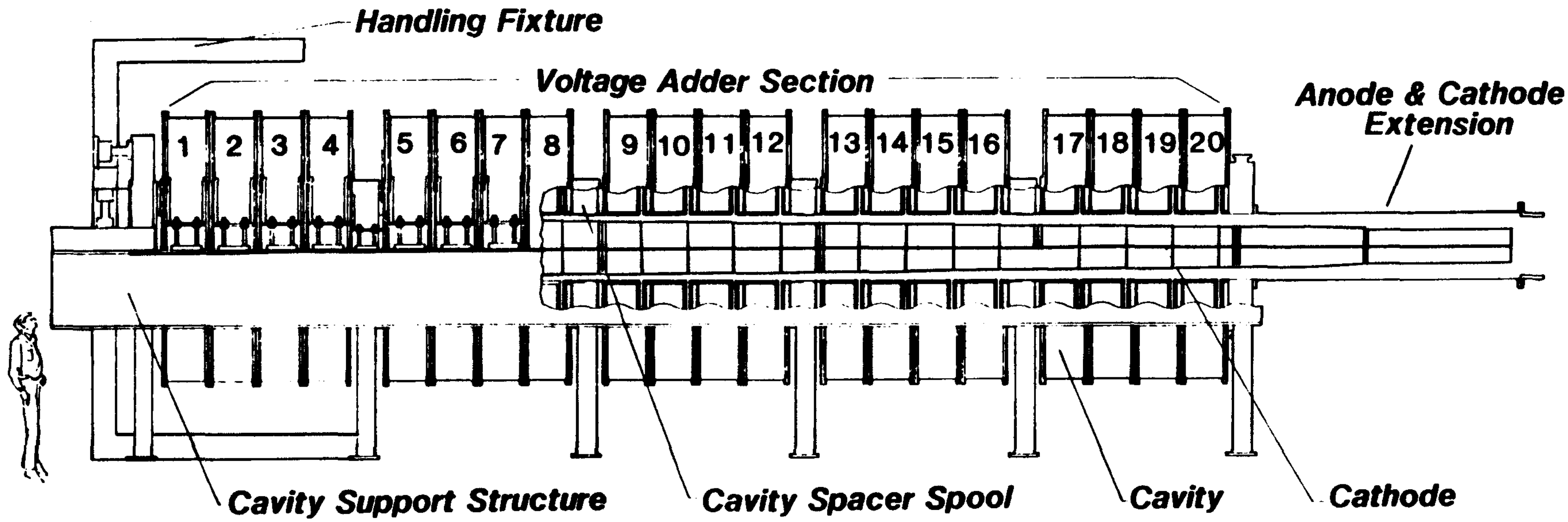

1. Cross section of the Hermes-III cavity adder and MITL.

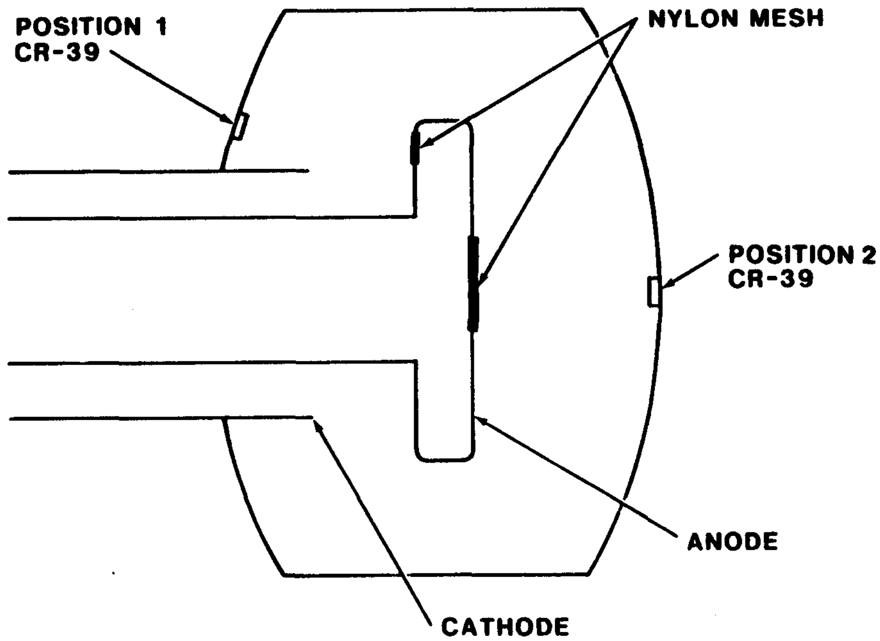

2. Electron beam diode

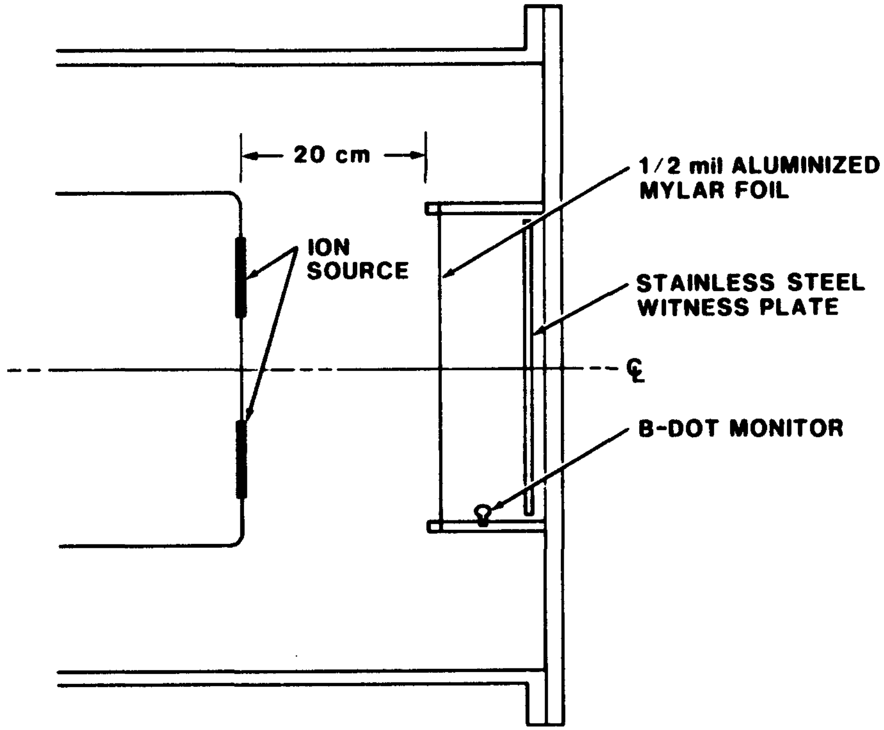
20 cm
ION
SOURCE
1/2 mil ALUMINIZED
MYLAR FOIL
STAINLESS STEEL
WITNESS PLATE
B-DOT MONITOR

3. Ion diode

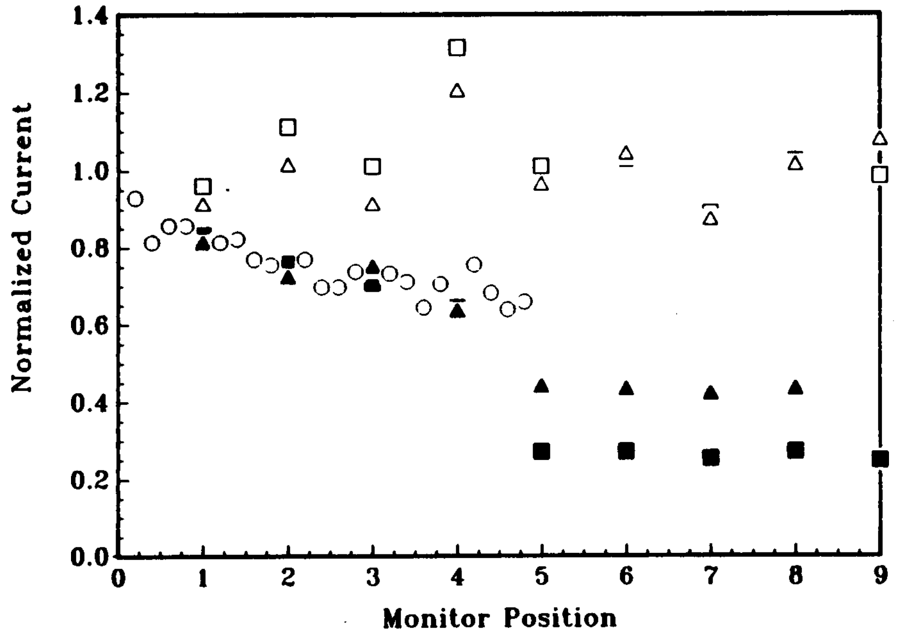

4. Normalized total and boundary currents for high voltage (squares) and low voltage (triangles) shots. Position 5 is just beyond the adder. The cavity currents (circles) match the bound current in the adder section.

5. Electron trajectory maps from MAGIC at 22 ns into the full-voltage, realistic-pulse Hermes-III simulation contrast the injected flow with the Insulated-Indigenous-Flow of the final MITL. Both flows are present in the simulation and together comprise the Full-Gap-Flow.

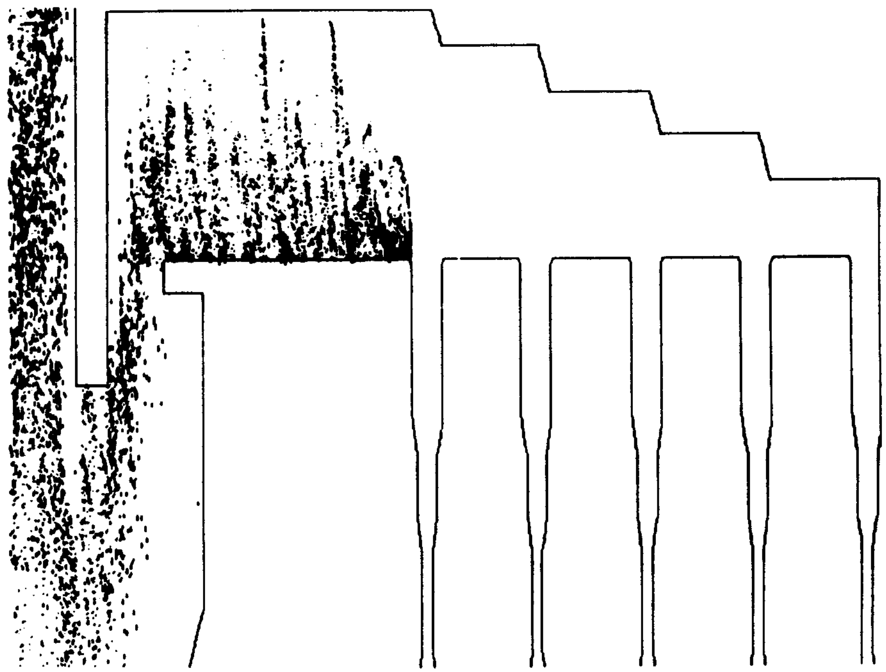

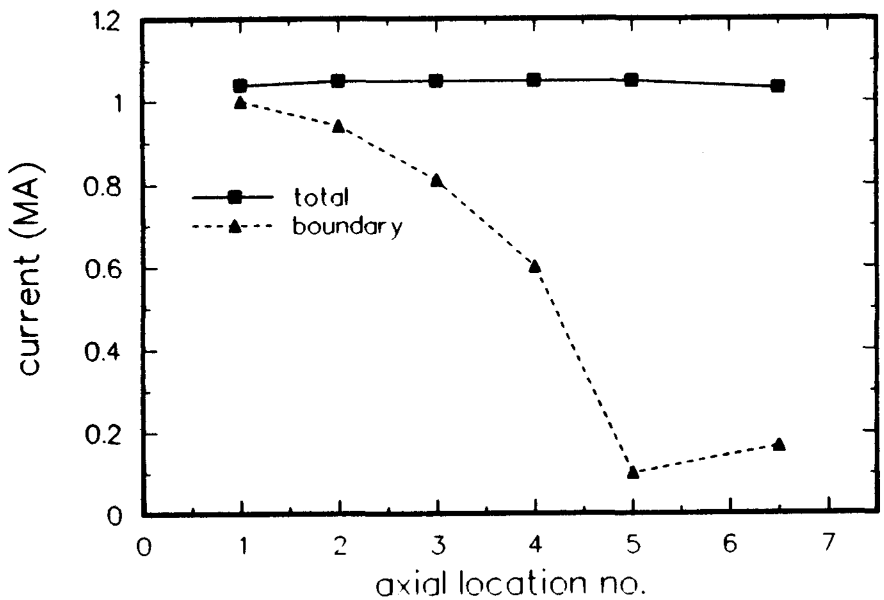

6. Plot of mid-pulse total and boundary currents vs. axial position from the full-voltage Hermes-III simulation. The location numbers correspond to those of the experiment.

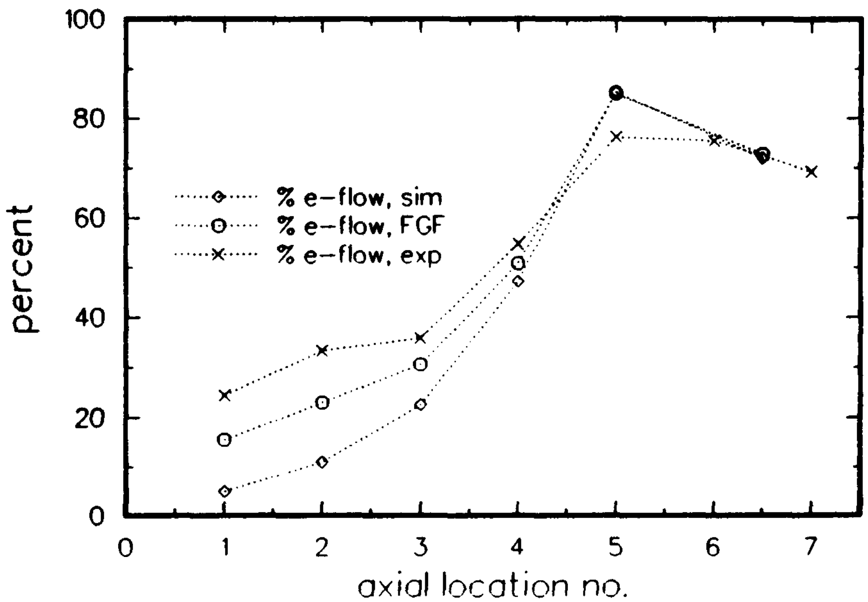

7. Comparison of full-voltage Hermes-III electron flows from simulation, shot 619, and FGF model.

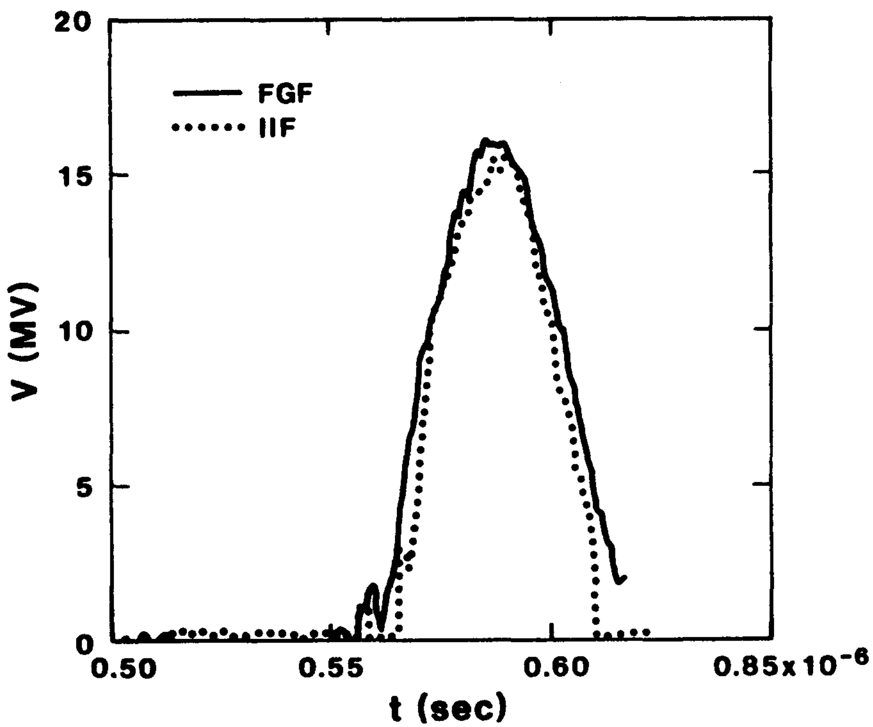

8. Comparison of calculated voltages for Hermes shot 619. The IIF voltage was calculated from cathode currents just upstream and downstream of the 20th feed; the FGF from the anode and cathode currents just downstream of the 20th feed.